Laserbasierte Charakterisierung der Spray- und Verdampfungszonen von Tropfen in einem Spray für die Flammensprühpyrolyse

Laser-based investigation of the spray evaporation of drops in a spray for flame spray pyrolysis

Malte F.B. Stodt[1,2], Udo Fritsching[1,3], Johannes Kiefer[2]
[1] Leibniz-Institut für Werkstofforientierte Technologien – IWT, Badgasteiner Str. 3, 28359 Bremen
[2] Technische Thermodynamik, Universität Bremen, Badgasteiner Str. 1, 28359 Bremen
[3] Mechanische Verfahrenstechnik, Produktionstechnik, Universität Bremen, Bibliothekstraße 1, 28359 Bremen

Flammensprühpyrolyse, Sprays, Globale Regenbogenrefraktometrie
Flame spray pyrolysis, spray combustion, global rainbow refractometry

Abstract
In flame spray pyrolysis (FSP), the precursor release from drops into the gas phase plays a key role for the morphology, size, and purity of crystalline metal oxide nanoparticles. The drop sizes as well as the drop life time are important parameters to control the particle formation and final product properties. In this work, the global rainbow refractometry technique is applied to a non-reactive ethanol spray with drops as small as 1-50 µm to investigate both, drop size distribution and averaged drop temperatures. The experimental global rainbow patterns are fitted to Lorenz-Mie theory (LMT) using the Rosin-Rammler-Sperling-Bennett (RRSB) distribution law. The results show an excellent agreement between the global rainbow experiment and LMT. The obtained drop size distributions show mean drop sizes in the range of 12 – 28 µm and drop temperatures from -2.9 – 3.6 along the central spray axis.

Introduction
The gas phase synthesis of functional nanoparticles by flame spray pyrolysis (FSP) has proven to be a promising and versatile production route allowing for a fast and scalable one-step particle synthesis (Kammler, Mädler, & Pratsinis, 2001; Mädler, Kammler, Mueller, & Pratsinis, 2002). FSP is capable of producing highly pure crystalline metal oxide nanoparticles with production rates of several kg/h (Mueller, Mädler, & Pratsinis, 2003) at an industrial scale. The product properties, such as crystallinity, particle size, and composition can be tailored by adjusting the relevant process parameters, e.g. the composition of precursor and solvent solution and the gas-to-liquid mass ratio (GLMR), among others.
FSP involves the atomization of the precursor and solvent solution using external mixing twin-fluid nozzles that consist of a coaxial dispersion gas (O_2) supply and a central capillary tube for the supply of the spray solution. The continuous ignition of the spray is achieved using a concentrically arranged premixed flat flame (CH_4 + O_2). A co-flow of air stabilizes the spray flame and provides stable boundary conditions. Depending on the physical properties of the precursor/solvent combination and the GLMR, the spray combustion leads to an intense heat release giving rise to gas phase temperatures of T > 2000 K. During the combustion, the gaseous precursor material nucleates to form primary nanoparticles which undergo particle growth

mechanisms, e.g. coalescence, coagulation, to form agglomerates and aggregates in the size of several hundreds of nanometres.
Within a DFG-funded Priority Programme (SPP1980) in Germany, a new standardized burner, called the SpraySyn-burner, has recently been introduced (Schneider et al., 2019). A detailed characterization of the spray formation, drop dynamics and flow conditions can be found in (Bieber, Tischendorf, Schmid, Reddemann, & R., 2019; Martins, Kirchmann, Kronenburg, & Beyrau, 2020; M. F. B. Stodt, Kiefer, & Fritsching, 2020). In our previous work (M. F. B. Stodt et al., 2020), the occurrence of micro-explosions (µ-explosions) was observed. These µ-explosions have also been investigated with similar precursor solutions in single drop experiments (Rosebrock, Wriedt, Mädler, & Wegner, 2016). They originate from a fast evaporation of the volatile solvent at the drop surface and an overheating of the volatile compound in the drop centre. The nucleation of vapour bubbles and their subsequent expansion leads to the formation of intense drop disruptions forming secondary drops. In FSP, phase Doppler anemometry (PDA) experiments have shown the formation of distinct bimodal drop size distributions (DSD) and an increased spray evaporation as a result of µ-explosions. Spatially resolved axial drop velocity and drop size correlations (u_D/d_D) emphasized the heterogeneous nature of turbulent spray flames, revealing local drop size dependent drop velocity differences as high as ~ 60 ms^{-1}. Not only is the high temperature residence time (HTRT) of the drops affected, but also the HTRT of the particles is influenced. Buss et al. (Buss, Noriler, & Fritsching, 2020) could show that the HTRT is of significant relevance for the final particle size distribution as short HTRT favour the synthesis of rather homogeneous particles. Besides these findings, the drop heating and spatial evolution of drop temperature during FSP still remains an open question. In our prior work (M. F. B. Stodt, Kiefer, & Fritsching, 2019) we investigated the group combustion modes of an ethanol spray flame and we could show that external and internal group combustion effects take place in the flame of the SpraySyn burner. To what extent these group combustion effects influence the evaporation kinetics of drop clouds in dense sprays is, however, yet to be investigated.
The experimental investigation of drop temperatures in sprays is still a challenging field of research. In general, sophisticated laser-based measurement techniques are used to obtain insights into the drop temperatures of sprays, for example laser-induced fluorescence (LIF) (Prenting, Dzulfida, Dreier, & Schulz, 2020) , Raman spectroscopy (Müller, Grünefeld, & Beushausen, 2000) or global rainbow refractometry (GRR) (Promvongsa et al., 2017; Saengkaew, 2005; M.F.B. Stodt, Wriedt, Kiefer, & Fritsching, 2021; Van Beeck, Giannoulis, Zimmer, & Riethmuller, 1999).
In the following, we utilize the GRR technique to experimentally investigate the applicability of GRR to non-reactive sprays with drop sizes as small as 1 - 30 µm. Contrary to the primary rainbows of single drops (C. Li, Lv, Wu, Wu, & Tropea, 2020; H. Li, Rosebrock, Wriedt, & Mädler, 2017), the superposition of multiple rainbows leads to a vanishing of the ripple structure and the airy fringes and to the formation of a broad primary rainbow. The shape and angular position of the rainbow is dependent on the drop sizes and the refractive index inside the probe volume. Local information about drop temperatures would give valuable insights into the evaporation of ethanol drops in a cold and reactive spray.

Materials and Methods

The experiments are carried out using the SpraySyn burner, which is mounted on a 2D traverse (Dantec Dynamics). The spray solution is supplied using a high-precision syringe pump (KD Scientific Gemini 88, Holliston, MA) and introduced into the burner *via* a capillary tube (inner diameter = 0.4 mm; outer diameter = 0.7 mm). The dispersion gas is introduced by a coaxial annular gap with an outlet diameter of 1.5 mm. In the outer region of an installed sinteredbrass plate co-flow (pressurized and filtered air) is operated to stabilize the spray and to ensure constant boundary conditions. The gas flow rates of the dispersion gas and the co-flow are controlled using mass flow controllers (EL-Flow, Bronkhorst). Ethanol (ethanol absolute, VWR Chemicals) was used without further purification. The ethanol feed rate was set to 2 mL min^{-1} and the oxygen dispersion gas flow was 10 standard litres min^{-1}, which results in a gas-to-liquid-mass-ratio of GLMR = 9.

Global Rainbow Refractometry

The experimental setup is shown in Fig. 1. The GRR experiments are conducted using a continuous wave Nd:YAG laser with a wavelength of λ = 532 nm (05-01 Cobolt). The scattered light from the drops is collected using the two lenses L_1 and L_2 (focal length f_1 = 100 mm, f_2 = 80 mm). L_1 is positioned at a distance of 150 mm from the measurement volume for a scattering range of $\Delta\theta$ = 16°. In the image plane of lens L_1, a pinhole (diam. 1 mm) is placed to select the measurement volume. Lens L_2 focusses the scattered light onto the linear array CCD camera (DALSA, Spyder 3). The angular calibration of stray light and CCD camera is performed using a rotational mirror that directs the unperturbed laser light on the camera. The accuracy of the rotational mirror is 1/60°. The GRR experiments were performed along the axial centre line of a cold ethanol spray for different heights above the burner (HAB).

With the global rainbow pattern being both, sensitive to the shape of the drop size distribution (DSD) and the refractive index (M.F.B. Stodt et al., 2021), the DSD and the refractive index are computed and fitted simultaneously using LMT to experimental rainbows. This approach is straightforward, since information about both, DSD and temperatures in sprays, can be determined by a single global rainbow pattern. The rainbow scattering patterns are simulated for single drops individually and then superposed.

The DSDs are described by a continuous function assuming a Rosin-Rammler-Sperling-Bennet (RRSB) distribution with the spread parameter σ and the location parameter $d_{p,RRSB}$ (63.2% of the drops are smaller) to be adjusted. Owing to the complex nature of the correlation between the stray light pattern and the drop size and drop temperatures, typical nonlinear optimization solver (e.g. Levenberg Marquardt) reach their limits finding the global maximum of the problem. Genetic algorithms have proven to be, despite their disadvantageous computational expense, a powerful tool for complex global optimization problems. In this work, the data is fitted using a genetic algorithm (ga, Matlab 2019b) with the following objective function *OF*

$$OF = \sum_{i=1}^{pix} \left(\frac{I_{exp} - I_{LMT}(n, \sigma, d_{p,RRSB})}{I_{exp}} \right)^2$$

where I_{exp} and I_{LMT} represent the normalised light scattering intensity of the experiment and LMT simulations for each pixel position *pix*, respectively.

Finally, the drop temperature is derived using a refractive index and temperature correlation for ethanol at a wavelength of λ = 532 nm, that is measured using an Abbe refractometer. The error of the refractive index measurement, caused by the accuracy of the thermocouple (ΔT = 0.2 K), is estimated by a gaussian error propagation with Δn = 8.1*10^{-5}.

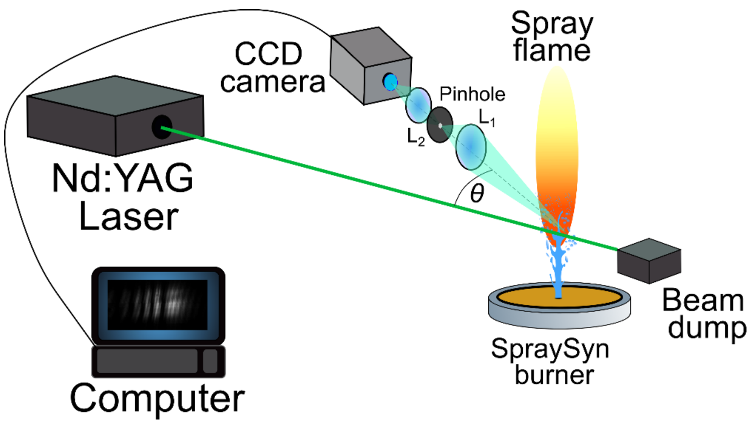

Figure 1: Schematic of the experimental setup for GRR measurements.

Results

Calibration:

The refractive index and temperature correlation for pure ethanol at a wavelength of λ = 532 nm is shown in Fig. 2a. The temperature range was limited to 23°C < T < 65°C by the thermostat and the boiling temperature T_b of ethanol (T_b = 78°C). The linear regression with a R^2 coefficient of R^2 = 0.999 shows a perfect linear relationship between the temperature and refractive index for the whole investigated temperature range.

The calibration of the pixel and angular position of the stray light is performed using a rotational mirror positioned in the measurement volume of the experimental setup. The measurement volume has been previously fixed by the intersection with a second laser beam. The principal laser beam is directed and focused on the CCD and the angle and pixel is determined. The laser beam intensity (P = 50 mW) is further reduced using an optical density filter (OD = 5) to be lower the damage threshold of the CCD sensor. The scale-reading accuracy of the rotational mirror is 1/60°. The linear relationship of the pixel number and angular position of the setup is shown in Fig. 2b for an angular range of 139° < θ < 155°.

Global Rainbow Refractometry

Figure 3a displays the raw image of a global rainbow pattern of a non-reactive ethanol spray. The vertical axis represents the time (in total 1.5 ms) and the horizontal axis the scattering angle of the scattered light. The uniform and stable evolution of the intensity along the time indicates a uniform temperature distribution and stable size and shape of the drops inside the measurement volume. The scattering pattern is integrated over time and normalised by the maximum of the rainbow pattern.

Figure 3b displays the evolution of normalised global rainbows of an ethanol spray for locations from 20 mm ≤ HAB ≤ 70 mm. The ripple structure, as well as airy fringes that are observed in rainbows of single drops, are as abovementioned vanished by the superposition of the rainbows of numerous drops. As can be observed here, the global rainbows experience a shift towards smaller scattering angles and a narrowing of the rainbow pattern with increasing distance from the nozzle exit which might be caused by a decrease in refractive index and changes of the DSD.

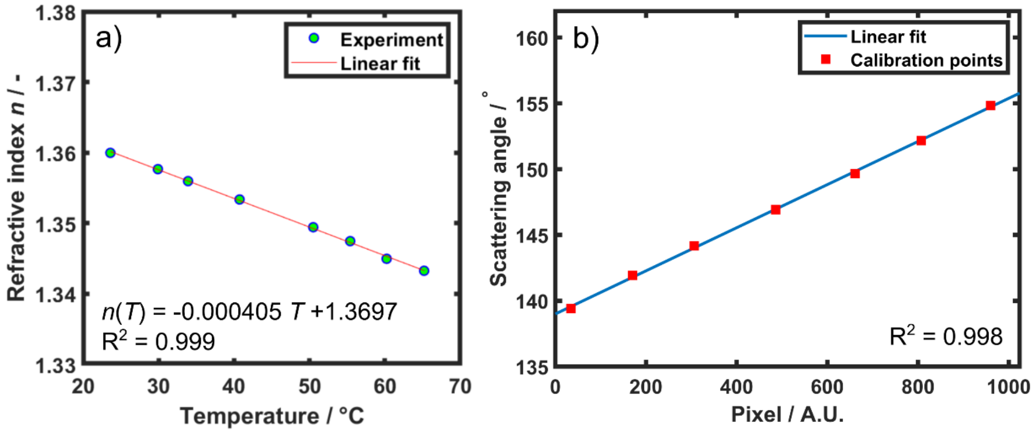

Figure 2: a) Correlation of the refractive index *n* and the temperature *T* of ethanol at λ = 532 nm; b) Calibration of the angle of light scattering and the pixel position on the line camera.

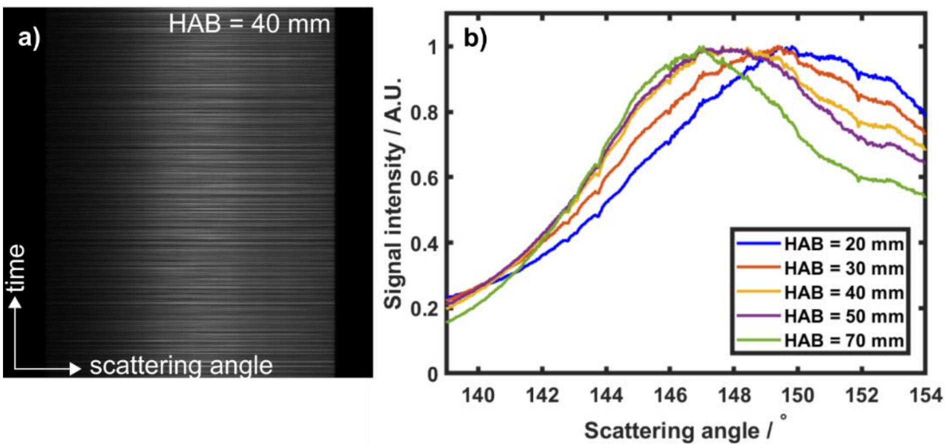

Figure 3: a) Light scattering pattern in a non-reactive ethanol spray on the axial centre line at HAB = 40 mm; b) The axial evolution of the normalised primary rainbow pattern of the spray of the SpraySyn nozzle.

A comparison of the fitted rainbow pattern and the experimental data is shown in Fig. 4. The results show a good agreement between experiment and LMT. Furthermore, the angular positions of the global rainbow maxima are indicated. Their angular positions as a function of HAB is displayed in Fig. 5a and shows an exponential decay for the range of 20 mm ≤ HAB ≤ 70 mm. This behaviour is mainly attributed to the changes in the shape of the DSD along the axial centre line of the spray, that are shown in Fig. 5b.

As shown in our previous work (M.F.B. Stodt et al., 2021), the increase of the mean drop due to the fast evaporation of small drops and to the radial deflection of preferably small drops with low inertia leads the global rainbow maximum positions to be shifted towards lower angles.

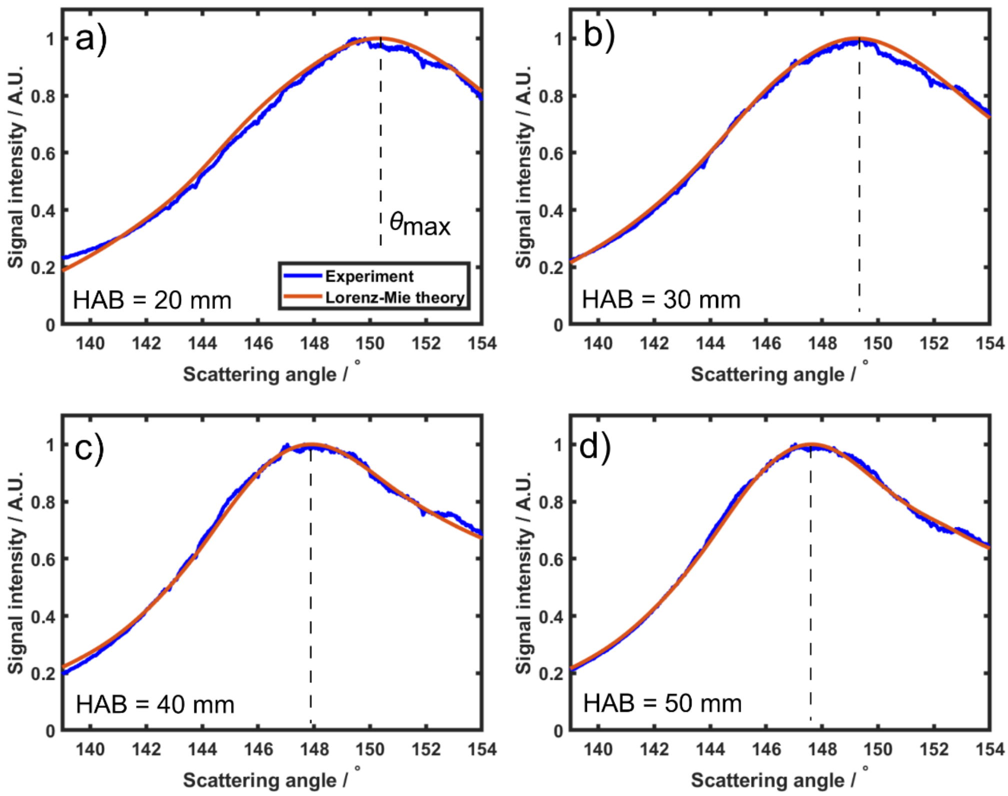

Figure 4: Experimental rainbow patterns with corresponding simulated LMT rainbows. The dashed lines indicate the angular position of the global rainbow maximum. a) HAB = 20 mm; b) HAB = 30 mm; c) HAB = 40 mm; d) HAB = 50 mm.

Figure 6 shows the evolution of the arithmetic mean diameter (d_{mean}) calculated from the obtained RRSB DSD from the GRR experiments. The lowest mean drop diameter is observed at HAB = 20 mm with d_{mean} = 12.9 µm. Owing to the radial deflection and evaporation of the smallest drops, the mean diameter increases with increasing distance to the nozzle up to d_{mean} = 28.0 µm at HAB = 70 mm. The rather small drop sizes and low feed rate (2 mL min^{-1}) reduce the probability of significant drop collisions that might cause a shift towards larger mean drop sizes. The trend of increasing mean diameters along the centre line, as well as the order of magnitude of the obtained mean diameter, are consistent with PDA measurements in the literature (Bieber et al., 2019; Heine & Pratsinis, 2005; M. F. B. Stodt et al., 2020).

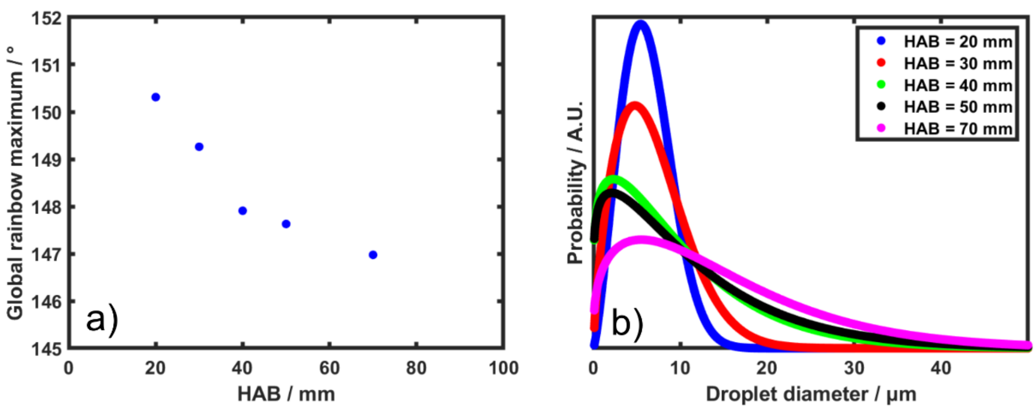

Figure 5: a) Evolution of the angular positions of the global rainbow maxima θ_{max} from LMT; b) Probability diagram of the evolution of the RRSB distributions.

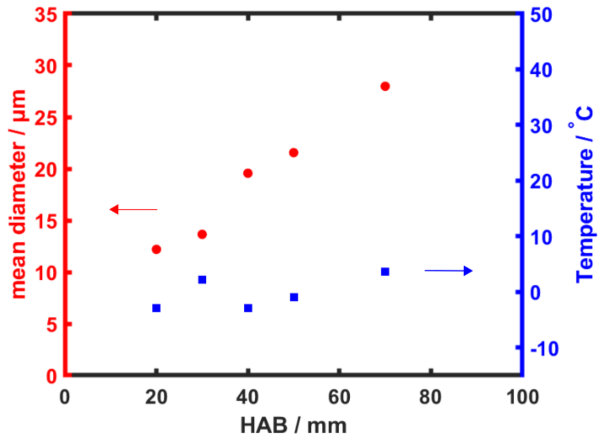

Figure 6: The arithmetic mean diameter d_{mean} and the axial evolution of mean drop temperature along the axial centre line of the spray.

The mean drop temperature is derived from the fitted refractive indices of the GRR signals using the abovementioned temperature and refractive index correlation. As can be observed in Fig. 6 the drops experience a significant temperature drop during the primary and secondary atomization from room temperature down to T = -2.9 °C at HAB = 20 mm. This intense temperature drop is caused by the fast drop evaporation in the highly turbulent jet, that is mainly driven by convection. The large surface to volume ratio of the relatively small drops further accelerate the temperature drop in the liquid phase. Along the centre line, a slight increase in drop temperature is observed up to T = 3.6 °C at HAB = 70 mm. It is likely that this increase in temperature can be attributed to local drop size dependent temperature differences. While smaller drops possess a larger surface to volume ratio, they tend to evaporate and cool much faster than bigger drops. The slight increase towards larger mean drop diameter downstream by the radial deflection of small drops results in an increase of the mean drop temperature.

Conclusions

The global rainbow refractometry technique has been applied for the simultaneous determination of the drop size distributions and the averaged refractive index of the liquid phase in the sample volume of a non-reactive ethanol spray. The corresponding liquid phase temperature has been derived using a temperature/refractive index correlation for the underlying laser wavelength of 532 nm. The obtained results revealed a decrease of the angular position of the global rainbow maxima with increasing distance to the nozzle. This effect might mainly be driven by the radial deflection of smaller drops and an increase of liquid phase temperature along the spray axis. The drop sizes are determined to be in the range from 1 – 50 µm with mean diameters in the range of 12 –28 µm. The averaged drop temperatures lay between -2.9 and 3.6 °C. The present approach of simultaneously fitting the drop size distribution and the refractive index of the liquid phase is a straightforward technique that enables the spatial investigation of sprays with drops as small as several microns. In future work, the GRR technique will be applied to reacting sprays to get insights into the drop evaporation during flame spray pyrolysis.

Acknowledgements

We acknowledge financial support from the Deutsche Forschungsgemeinschaft within the priority program SPP 1980 SPRAYSYN under Grants KI 1396/6-2 and FR 912/42-2.

Literature

Bieber, M., Tischendorf, R., Schmid, H. J., Reddemann, & R., M. K. (2019). Influence of Precursor Concentration on Spray and Particle Formation in Flame Spray Pyrolysis. *Proc. 29th Europ. Conf. Liq. Atomization Spray Syst.*

Buss, L., Noriler, D., & Fritsching, U. (2020). Impact of Reaction Chamber Geometry on the Particle-Residence-Time in Flame Spray Process. *Flow Turb. Combust., 105*(4), 1055-1086.

Heine, M. C., & Pratsinis, S. E. (2005). Droplet and particle dynamics during flame spray synthesis of nanoparticles. *Ind. Eng. Chem. Res., 44*(16), 6222-6232.

Kammler, H. K., Mädler, L., & Pratsinis, S. E. (2001). Flame synthesis of nanoparticles. *Chem. Eng. Technol., 24*(6), 583-596.

Li, C., Lv, Q., Wu, Y., Wu, X., & Tropea, C. (2020). Measurement of transient evaporation of an ethanol droplet stream with phase rainbow refractometry and high-speed microscopic shadowgraphy. *Int. J. Heat Mass Transfer, 146*, 118843.

Li, H., Rosebrock, C. D., Wriedt, T., & Mädler, L. (2017). The effect of initial diameter on rainbow positions and temperature distributions of burning single-component n-Alkane droplets. *Journal of Quantitative Spectroscopy and Radiative Transfer, 195*, 164-175.

Mädler, L., Kammler, H., Mueller, R., & Pratsinis, S. E. (2002). Controlled synthesis of nanostructured particles by flame spray pyrolysis. *J. Aerosol Sci., 33*(2), 369-389.

Martins, F. J., Kirchmann, J., Kronenburg, A., & Beyrau, F. (2020). Experimental investigation of axisymmetric, turbulent, annular jets discharged through the nozzle of the SPP1980 SpraySyn burner under isothermal and reacting conditions. *Exp. Thermal Fluid Sci., 114*, 110052.

Mueller, R., Mädler, L., & Pratsinis, S. E. (2003). Nanoparticle synthesis at high production rates by flame spray pyrolysis. *Chem. Eng. Sci., 58*(10), 1969-1976.

Müller, T., Grünefeld, G., & Beushausen, V. (2000). High-precision measurement of the temperature of methanol and ethanol droplets using spontaneous Raman scattering. *Appl. Phys. B, 70*(1), 155-158.

Prenting, M. M., Dzulfida, M. I. B., Dreier, T., & Schulz, C. (2020). Characterization of tracers for two-color laser-induced fluorescence liquid-phase temperature imaging in sprays. *Exp. Fluids, 61*(3), 1-15.

Promvongsa, J., Vallikul, P., Fungtammasan, B., Garo, A., Grehan, G., & Saengkaew, S. (2017). Multicomponent fuel droplet evaporation using 1D Global Rainbow Technique. *Proceed. Combust. Inst., 36*(2), 2401-2408.

Rosebrock, C. D., Wriedt, T., Mädler, L., & Wegner, K. (2016). The role of microexplosions in flame spray synthesis for homogeneous nanopowders from low-cost metal precursors. *AIChE J., 62*(2), 381-391.

Saengkaew, S. (2005). *Study of spray heat up: on the development of global rainbow techniques.* Rouen,

Schneider, F., Suleiman, S., Menser, J., Borukhovich, E., Wlokas, I., Kempf, A., . . . Schulz, C. (2019). SpraySyn—A standardized burner configuration for nanoparticle synthesis in spray flames. *Rev. of Scientific Instruments, 90*(8), 085108.

Stodt, M. F. B., Kiefer, J., & Fritsching, U. (2019). Ethanol droplet formation, dynamics and combustion mode in the flame of the SpraySyn-nozzle. *Exp. Fluids, 60*(8), 125.

Stodt, M. F. B., Kiefer, J., & Fritsching, U. (2020). Drop Dynamics in Heterogeneous Spray Flames for Nanoparticle Synthesis. *Atomization Sprays, 30*(11).

Stodt, M. F. B., Wriedt, T., Kiefer, J., & Fritsching, U. (2021). Theoretical investigation of global rainbow refractometry in spray combustion of polydisperse microdroplets. *J. Modern Optics, 68*(5), 259-266.

Van Beeck, J., Giannoulis, D., Zimmer, L., & Riethmuller, M. (1999). Global rainbow thermometry for droplet-temperature measurement. *Opt. lett., 24*(23), 1696-1698.